Electronic Supplementary Material (ESI) for Journal of Materials Chemistry A.

Supplementary Information

Relating open-circuit voltage losses to the active layer morphology and contact selectivity in organic solar cells

Zheng Tang[a,b], Jing Wang[a], Armantas Melianas[b], Yang Wu[c], Renee Kroon[d], Weiwei Li[e], Wei Ma[c], Mats R. Andersson[f], Zaifei Ma[a]*, Wanzhu Cai[b]*, Wolfgang Tress[g]*, Olle Inganäs[b]*

a. State Key Laboratory for Modification of Chemical Fibers and Polymer Materials, Center for Advanced Low-dimension Materials, College of Materials Science and Engineering, Donghua University, Shanghai, 201620, P. R. China

b. Biomolecular and Organic Electronics, IFM, and Center of Organic Electronics, Linköping University, SE-581 83, Linköping, Sweden

c. State Key Laboratory for Mechanical Behavior of Materials, Xi'an Jiaotong University, Xi'an 710049, P. R. China

d. Department of Chemistry and Chemical Engineering, Chalmers University of Technology, 41296, Göteborg, Sweden

e. Beijing National Laboratory for Molecular Sciences, CAS Key Laboratory of Organic Solids, Institute of Chemistry, Chinese Academy of Sciences, Beijing 10090, China

f. Flinders Institute for NanoScale Science and Technology, Flinders University, Sturt Road, Bedford Park, 5042, Australia

g. Laboratory of Photomolecular Science, Institute of Chemical Sciences, Engineering, École Polytechnique Fédérale de Lausanne, 1015 Lausanne, Switzerland

E-mail: mazaifei@dhu.edu.cn; wanzhu.cai@liu.se; wolfgang.tress@epfl.ch; oling@ifm.liu.se

Characteristic curves and internal quantum efficiency of PTNT:PC$_{71}$BM solar cells

As shown in Fig. S1, even at -5 V, the extracted photocurrent does not reach the theoretical maximum predicted by a transfer matrix model ($J_{SC\text{-}max}$ = 10.5 mA cm^{-2}) for all of the solar cells, indicating that the device internal quantum efficiencies (IQEs) are much lower than 100%.

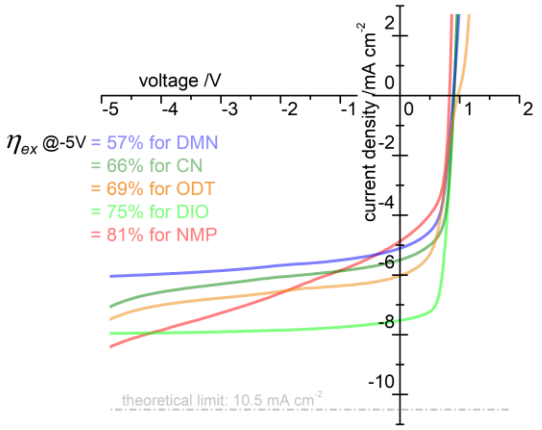

Fig. S1. JV characteristics of solar cells with active layers cast from the different solvent additives and the theoretical maximum photocurrent for these solar cells, calculated using a transfer matrix model. η_{ex} estimated by taking the ratio between the current extracted at -5V and the theoretical maximum current are also given. Note that current extraction in the solar cell cast from NMP is voltage dependent, even at -5 V. This indicates that . η_{ex} is underestimated for the solar cell cast from NMP.

IQE of an OSC can be expressed as

$$IQE(V) = \eta_{ex} \cdot \eta_{CT} \cdot \eta_{free}(V)$$

where η_{ex} is the conversion efficiency of a polymer or PC$_{71}$BM exciton to a CT state exciton, which is directly related to the degree of D/A phase separation in the BHJ active layer, but independent of the applied voltage bias; η_{CT} is the conversion efficiency of CT state excitons to free charge carriers, and $\eta_{free}(V)$ is the extraction efficiency of free charge carriers, which depends on the applied voltage bias V and is lower than 100% due to bimolecular recombination.

The large energetic driving force in the PTNT:PC$_{71}$BM system ensures that η_{CT} is close to 100% regardless of the solvent additive used, and the relatively constant photocurrent extraction under reverse bias suggests η_{free} of close to 100% for the solar cells under reverse bias (except for the device based on NMP). This indicates that when the solar cells are under reverse bias, their IQE is mainly determined by η_{ex}. We estimate η_{ex} by taking the ratio between the photocurrent extracted at -5 V with the maximum achievable photocurrent, simulated with an optical transfer matrix model (using experimentally obtained dielectric functions for the materials used). Results are indicated in Fig. S1. The differences for solar cells cast from different additives are thus due to the changes in D/A phase separation: The highest and the lowest η_{ex} are obtained for the solar cells cast from NMP and DMN, respectively, indicating a finest and a coarsest morphology, in agreement with the previously discussed PL and GIWAXS measurements.

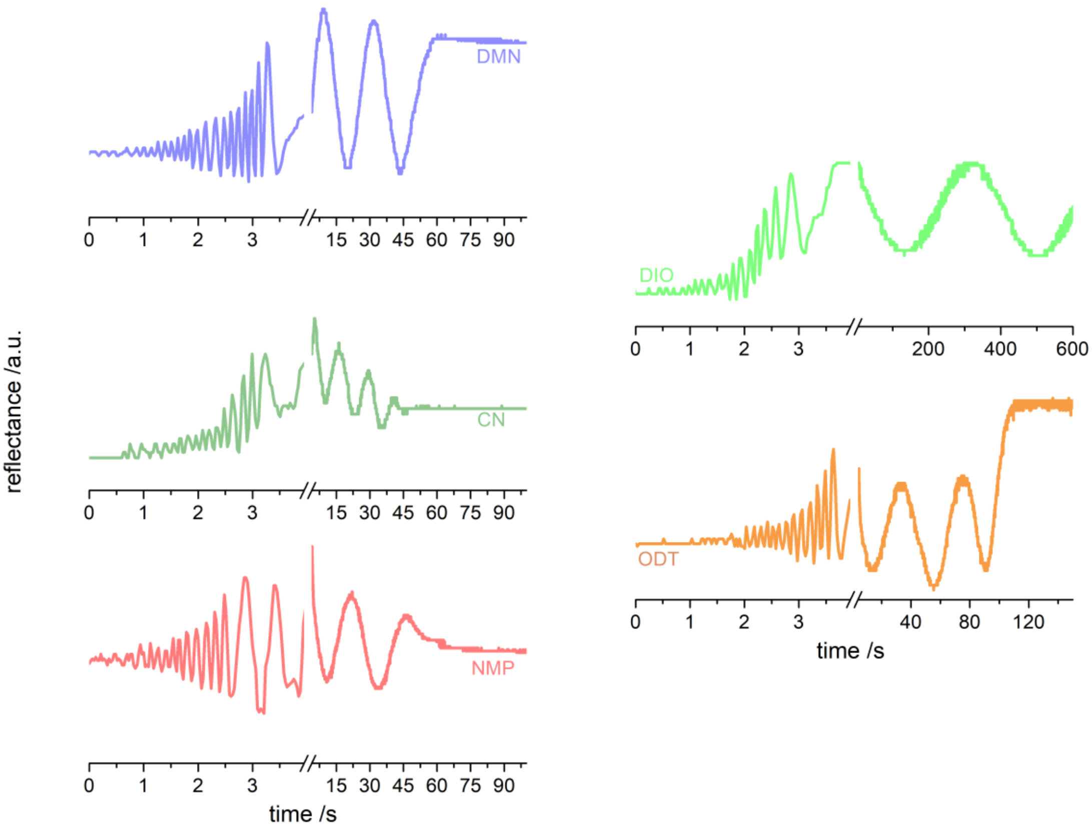

Fig. S2. Drying kinetics of the active layers cast (PTNT:PC$_{71}$BM 2:3) from o-xylene with different solvent additives. Specular reflectance is measured during film drying under LED illumination (wavelength ≈ 450 nm) as a function of time. Reflectance oscillations are induced due to changes in optical interference conditions during film drying, whereas the constant reflectance at later time scales indicates that the film is completely dry (except for the case of DIO). In all cases, two distinct drying kinetics are resolved, which are ascribed to the different evaporation rates of the host solvent o-xylene and the solvent additive. A much faster evaporation of o-xylene, with a removal time of ~4 s, is observed for all of the active layer systems, whereas the removal time for the different additives is significantly longer (note the x-axis breaks in the plots). The significantly higher oscillation frequency observed at the early time scale indicates a much faster thinning of the wet film upon o-xylene evaporation. However, the evaporation of the solvent additive, which controls the final stage of the drying kinetics, dictates the formation of phase separation.

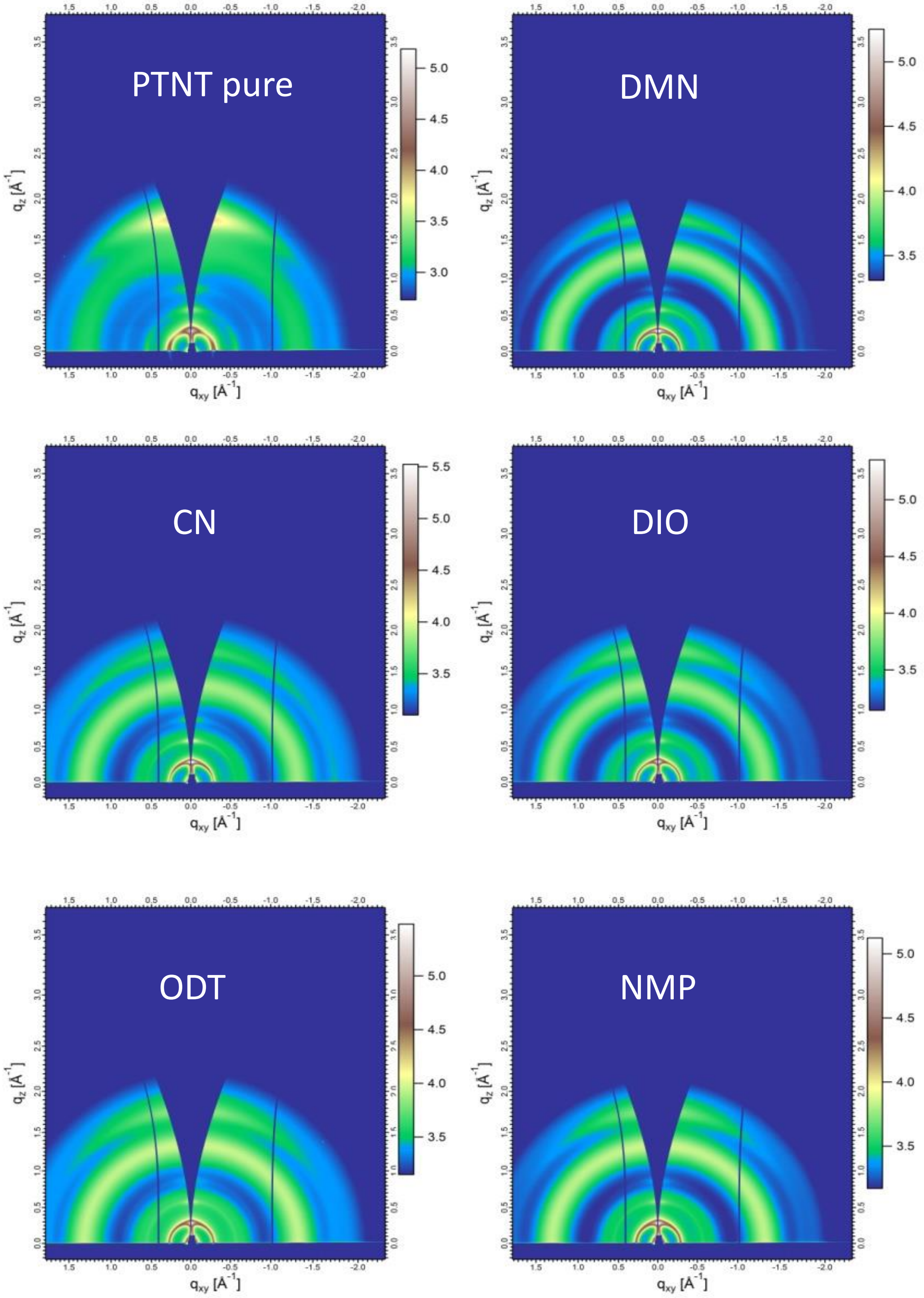

Fig. S3. 2D-GIWAXS images of a pure PTNT film and BHJ films cast from different solvent additives. Deposition conditions used for the films are the same as those used to fabricate the corresponding solar cell devices.

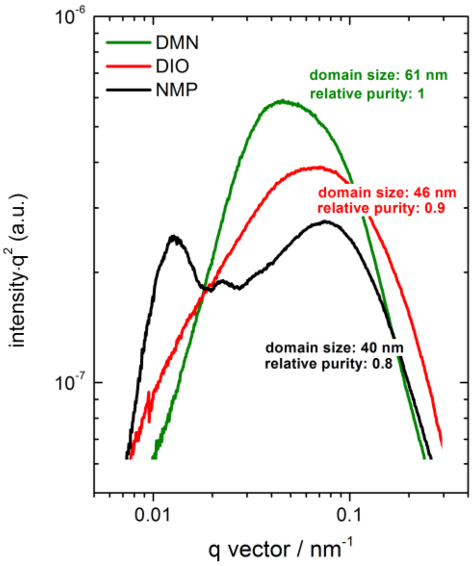

Fig. S4. RSoXS scattering profiles at 283 eV for BHJ films based PTNT:PC71BM cast from different solvent additives. Average domain size decreases from 61 nm for the film cast from DMN to 40 nm for the film from NMP. The results agree well with GIWAXS and PL measurements. Note that the first peak in the data from NMP (q~0.01 nm-1) originates from a high surface roughness, as confirmed by the AFM images shown below.

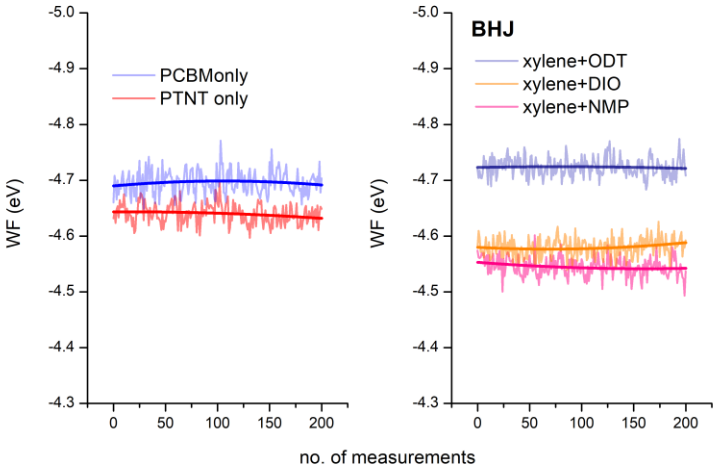

Fig. S5. The work function of pure PCBM, pure PTNT and the blend active layers cast from ODT, DIO, and NMP, measured by a Kelvin probe. The work function of PCBM and PTNT are ~-4.7 eV and ~-4.6 eV, respectively. The work function of the blend cast DIO or NMP is about -4.6 eV, and the work function of the blend cast from ODT is ~-4.7 eV. Note that the work function of the blend cast from DIO or NMP is higher than work function of pure $PC_{71}BM$, this is likely due to a slight change of the work function of PTNT in the blend.

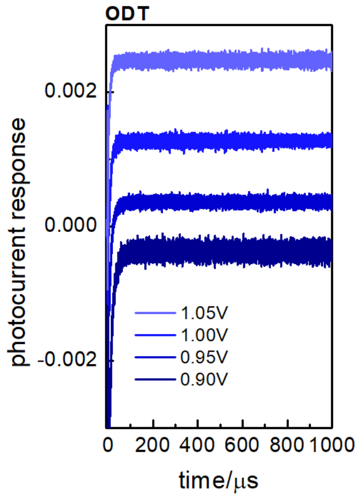

Fig. S6. Transient photocurrent of the solar cell based on ODT measured at the indicated bias voltages.

Table S1. Structural parameters of a pure PTNT film cast from o-xylene, and PTNT in BHJ films based on PTNT:$PC_{71}BM$ casted from o-xylene and different solvent additives. The peaks at $q \approx 1.4$ Å^{-1} are used for the estimate of CL_{PCBM}.

	d_{010}-spacing (Å)	**CL_{010} (Å)**	**d_{100}-spacing (Å)**	**CL_{100} (Å)**	**CL_{PCBM} (Å)**
DMN	3.6	54.81	22.0	264.64	26.84
CN	3.6	47.23	22.0	228.26	26.74
DIO	3.6	44.04	22.0	233.16	25.58
ODT	3.6	44.03	22.0	215.01	27.57
NMP	3.6	42.60	22.0	208.51	26.12

Table S2. EQE_{EL}, fit parameters for FTPS-EQE spectra and V_{OC} statistics over 12 devices for solar cells cast from different solvent additives.

	EQE_{EL}	**f /eV^2**	**λ /eV**	**E_{CT} /eV**	**V_{OC} /V**
NMP	5×10^{-8}	0.006	0.45	1.52	0.82±0.01
DMN	7×10^{-8}	0.002	0.39	1.52	0.89±0.01
CN	6.5×10^{-8}	0.002	0.38	1.51	0.90±0.01
DIO	7×10^{-8}	0.002	0.40	1.52	0.90±0.01
ODT	9×10^{-7}	0.002	0.40	1.51	0.97±0.02

Table S3. Parameters used in the one-dimensional numerical drift-diffusion simulations. The blend is simulated as an effective medium between metal electrodes. Contact selectivity is determined by the boundary conditions for the electron and hole currents. For modelling the JV characteristics of the ODT device under weaker illumination intensities, lower generation rates were used. For details on drift-diffusion simulations see Chapter 4 in Tress, W. *Organic Solar Cells*. **208,** (Springer International Publishing, 2014).

Effective band gap	1.5 /eV
Generation rate	$5x10^{21}$ /cm^{-3}s^{-1}
thickness	80 /nm
Electron mobility	$1x10^{-4}$ /cm^{2}V^{-1}s^{-1}
Hole mobility	$1.5x10^{-4}$ /cm2/Vs
Effective densities of states	$1x10^{20}$ /cm^{-3}
Dielectric constant	3
Bimolecular recombination rate constant	$2x10^{-10}$ /cm^{3}s^{-1}
Built-in potential	0.95 /V

Note: The generation rate is set to match the photocurrent. Bimolecular recombination rate constant, mobility and the built-in potential are determined by fitting the experimentally obtained S-shaped curve. Although it is possible to reproduce the S-kink and the current-voltage characteristic for the below V_{OC} range with comparable accuracy, by using a combination of a lower built-in potential with a higher charge carrier mobility, the simulated forward current (in the first quadrant of the JV plot) will be significantly different from that of the experimental result. Therefore, it is concluded that the selected parameter combination is the best-matching one.

Table S4. Performance parameters of the solar cells fabricated with different solvent additives.

	Voc /V	**Jsc mA cm^{-2}**	**FF**	**PCE /%**
NMP	0.82	4.87	0.57	2.26
DMN	0.9	5.11	0.57	2.65
CN	0.9	5.5	0.63	3.14
DIO	0.9	7.52	0.64	4.34
ODT	0.97	6.02	0.50	2.89

Note: PCE of the DIO based device is the highest, compared to that of the devices cast from other solvent additives. However, the DIO device performs worse than the most efficient solar cells based on PTNT reported in literature (J. Am. Chem. Soc. 136, 33, 11578-11581). This is mainly because the active layer used in this work is thinner (80 nm vs 200 nm) and the solar cell absorbs less light.